Experiments on the Scalar Structure of Turbulent $CO/H_2/N_2$ Jet Flames

R. S. BARLOW
Combustion Research Facility, Sandia National Laboratories, Livermore, CA 94551-0969

G. J. FIECHTNER, C. D. CARTER
Innovative Scientific Solutions, Inc., Dayton, OH 45440-3638

and

J.-Y. CHEN
Mechanical Engineering Department, University of California, Berkeley, CA 94720

Scalar and velocity measurements are reported for two turbulent jet flames of $CO/H_2/N_2$ (40/30/30 volume percent) having the same jet Reynolds number of 16,700 but different nozzle diameters (4.58 mm and 7.72 mm). Simultaneous measurements of temperature, the major species, OH, and NO are obtained using the combination of Rayleigh scattering, Raman scattering, and laser-induced fluorescence. Three-component laser-Doppler velocimetry measurements on the same flames were performed at ETH Zurich and are reported separately. This paper focuses on the scalar results but includes some limited velocity data. Axial profiles of mixture fraction, major species mole fractions, and velocity in these two flames are in close agreement when streamwise distance is scaled by nozzle diameter. However, OH mole fractions are lower and NO mole fractions are higher near the stoichiometric flame length in the larger flame due to the lower scalar dissipation rates and longer residence times. Turbulent flame measurements are compared with steady strained laminar flame calculations. Laminar calculations show remarkably close agreement with measured conditional means of the major species when all diffusivities are set equal to the thermal diffusivity. In contrast, laminar flame calculations that include the normal Chemkin treatment of molecular transport are clearly inconsistent with the measurements. These results suggest that turbulent stirring has a greater influence than molecular diffusion in determining major species concentrations at the flow conditions and locations considered in the present experiments, which begin at an axial distance of 20 nozzle diameters. Analysis of the conditional statistics of the differential diffusion parameter supports this conclusion, though some evidence of differential diffusion is observed. With regard to validation of turbulent combustion models, this data set provides a target that retains the geometric simplicity of the unpiloted jet flame in coflow, while including a chemical kinetic system of intermediate complexity between hydrogen flames and the simplest hydrocarbon flames. Aspects of the measurements, including Favre-averaged profiles, conditional statistics, mixture fraction pdf's, and departures from partial equilibrium, are presented and discussed in terms or their relevance to the testing of turbulent combustion submodels. The complete data are available on the World Wide Web for use in model validation studies.

INTRODUCTION

Detailed scalar and velocity data sets are essential for the process of testing and improving computational models for turbulent nonpremixed combustion. Laser diagnostics can provide nonintrusive measurements of the instantaneous velocities and species concentrations, and statistical information from such measurements may be used to evaluate a variety of modeling approaches. Despite the very productive history of laser diagnostics in combustion, the number of data sets available in the literature that are appropriate for the quantitative evaluation of fundamental aspects of turbulent combustion models is relatively small. It is important for such data sets to include well-defined boundary conditions and relatively simple geometric configurations. It is also important that both velocity and scalar measurements be available for the same flames. Multicomponent velocity measurements are preferable, as are multiscalar measurements that include minor species. Minor species, such as combustion intermediates, radicals, and pollutants, tend to be sensitive to the details of

*Corresponding author. E-mail: barlow@ca.sandia.gov

COMBUSTION AND FLAME 120:549–569 (2000)

Published by Elsevier Science Inc.

0010-2180/00/$–see front matter
PII S0010-2180(99)00126-1

interactions between fluid dynamics and chemical kinetics. Consequently, measurements of minor species can provide information on the fundamental nature of these interactions, and the prediction of minor species along with velocity, temperature, and major species constitutes a useful test of combustion models.

There are at least three detailed scalar and velocity data sets for hydrogen jet flames [1–4]. Model calculations of some of these flames have been compared [5–7], and it appears that state-of-the-art models are capable of yielding accurate calculations of such flames, including difficult details such as nitric oxide formation. The present paper focuses on simple, attached jet flames of 40% CO/30% H_2/30% N_2 (also referred to as syngas in the literature), which add a modest increment in chemical kinetic complexity, while retaining the simple geometry of the hydrogen jet flames. This study is part of a larger collaborative effort under the framework of the International Workshop on Measurement and Computation of Turbulent Nonpremixed Flames (TNF) [4] to develop a library of well-documented data sets that covers a progression in geometric and chemical kinetic complexity.

The fuel combination of carbon monoxide and hydrogen allows for the study of interactions of turbulent mixing and chemical reaction over a range of chemical time scales, including those associated with the binary reactions of the hydrogen–oxygen system, the oxidation of CO, the decay of OH through the three-body recombination reactions, and the thermal formation of nitric oxide. The flames considered here do not exhibit localized extinction or liftoff. Therefore, they can be addressed by a wide range of modeling approaches.

Reviews of the available experimental data sets on turbulent nonpremixed flames have been provided by Strahle [8], Faeth and Samuelsen [9], Drake and Kollmann [10], and more recently by Masri et al. [11]. Several experiments involving simultaneous multiscalar measurements based on Raman/Rayleigh or Raman/Rayleigh/LIF (laser-induced fluorescence) techniques have been conducted on flames having CO as a major fuel component. These include studies of piloted and bluff-body stabilized flames of CO/H_2/N_2 by Masri and Dibble [12] and Correa and Gulati [13, 14]. The paper by Masri et al. [15] on hydrogen jet flames diluted with CO_2 is closely related, in a chemical kinetic sense, because the CO_2 is partially converted to CO at high temperatures within the flame. These experimental studies have provided useful insights on turbulence–chemistry interactions, particularly with regard to differences in extinction behavior among flames of H_2, CO/H_2, and hydrocarbon fuels. However, they are of limited utility with regard to rigorous, quantitative testing of turbulent combustion models because of the lack of complementary information on the velocity field.

We believe that the present data set has sufficient completeness and accuracy to make it useful for quantitative testing of turbulent combustion models. Raman/Rayleigh/LIF experiments were conducted at Sandia and include simultaneous point measurements of temperature, N_2, O_2, CO, H_2, CO_2, H_2O, OH, and NO. Subsequently, through the collaborative framework of the TNF Workshop, three-component laser-Doppler velocity (LDV) measurements were undertaken at ETH Zurich, Switzerland, and those experiments are reported separately by Flury [16]. The present paper focuses on the scalar measurements and includes only limited velocity data. Complete scalar and velocity data, together with documentation on boundary conditions and experimental uncertainties, are available on the Internet [17].

The following sections provide a description of experimental methods for the scalar measurements and present results in several forms, including averaged profiles, conditional statistics, probability density functions (pdf's), and derived quantities related to differential diffusion, and partial equilibrium. Measured conditional means are compared with steady laminar flame calculations to extract insights on the relative importance of turbulent stirring and molecular diffusion in determining the scalar structure of these flames.

EXPERIMENTAL METHODS AND MEASUREMENT UNCERTAINTIES

Multiscalar experiments were conducted in the Turbulent Diffusion Flame (TDF) laboratory at

Sandia's Combustion Research Facility. The flow facility, diagnostic systems, and calibration procedures have been described in previous publications [18–20]. The combination of spontaneous Raman scattering and Rayleigh scattering was used to measure the major species concentrations (N_2, O_2, CO, H_2, CO_2, H_2O) and temperature. Linear LIF was used to measure the concentrations of OH and NO. Fluorescence signals were corrected on a shot-to-shot basis for variations in the Boltzmann fraction and collisional quenching rate, based on measured temperature and major species concentrations in the probe volume. Collisional quenching cross sections for OH and NO were based on the work of Paul et al. [21, 22]. Spatial resolution of the scalar measurements was roughly 0.75 mm.

A system for two-photon LIF of CO was also implemented for this study, and part of the original motivation for investigating turbulent $CO/H_2/N_2$ flames was to allow direct comparison of the CO fluorescence and CO Raman methods in flames with a wide range of CO concentrations and without interferences from hydrocarbons. However, the signal-to-noise ratio (SNR) for the CO LIF measurements in the turbulent $CO/H_2/N_2$ flames was worse than for the Raman measurements, even though the LIF technique showed superior SNR in cold flows and calibration flames. The reasons are not known at this time. Beam steering effects and the differences in spatial resolution (beam diameters) were considered as possible causes, but tests showed that results were insensitive to these effects. This excess noise problem is not observed in turbulent methane flames [23]. CO results included in this paper are from Raman scattering measurements.

The precision of the scalar measurements is represented Fig. 1, which shows results of processed data from a series of CO/H_2–air flat flames (50/50 fuel mixture) operated on a Hencken burner [19]. The symbols show mean temperature and species mole fractions from each operating condition of the burner, and each symbol is surrounded by an ellipse having major and minor axes of twice the standard deviations ($\pm\sigma$) of the scalar and the mixture fraction. The standard deviations in these calibrations may be used to estimate the contribution of random error (primarily shot noise) to the conditional fluctuations reported below. Representative values of precision are listed in Table 1 for specific flame conditions.

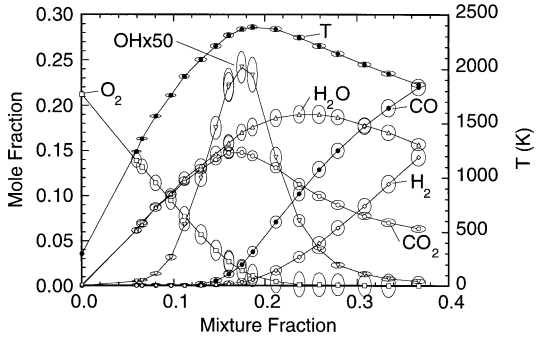

Fig. 1. Measured temperature and species mole fractions in the product gases above a series of CO/H_2–air calibration flames stabilized on a Hencken burner. Symbols show mean values from the Raman/Rayleigh/LIF data reduction process. Ellipses show standard deviations ($\pm\sigma$) for single-shot measurements of the scalars and for the resultant mixture fraction at each calibration condition.

Estimates of systematic uncertainties (absolute accuracy of averaged values) are also listed in Table 1 and are based on analysis of the calibration methods, repeatability of calibrations, considerations of calibration drift, allowances for greater uncertainties within the interpolated regions (approx. 900 K to 1600 K) of the calibration curves for H_2 and CO, and uncertainties in gas flow rates. Flow controllers were

TABLE 1

Standard Deviations of Scalars Measured in Flat Flames and Estimated Systematic Uncertainties

Scalar	σ (rms)	Conditions (mass fraction, T)	Systematic Uncertainty
T	1%	2140 K[a]	2%
Y_{N_2}	2%	0.73, 2140 K[a]	3%
Y_{H_2O}	5%	0.12, 2140 K[a]	3–5%
Y_{CO_2}	6%	0.14, 2140 K[a]	3–5%
Y_{CO}	13%	0.062, 2020 K[b]	5–10%
Y_{H_2}	17%	0.003, 2020 K[b]	5–10%
Y_{OH}	8%	0.0016, 2140 K[a]	10%
Y_{NO}	10%	8 ppm, 1760 K[c]	10–15%

[a] Premixed CH_4/air, ϕ = 0.96, uncooled (Hencken) burner.

[b] Premixed CH_4/air, ϕ = 1.27, uncooled (Hencken) burner.

[c] Premixed $CH_4/O_2/N_2$, ϕ = 0.72, cooled (McKenna) burner.

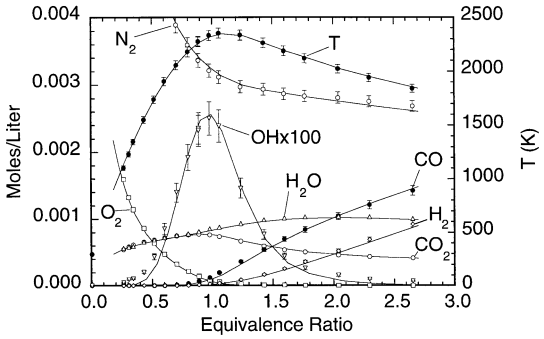

Fig. 2. Processed mean values of temperature and concentration in the CO/H_2–air Hencken-burner flames. Error bars show estimated systematic uncertainties, as listed in Table 1. Solid lines connect nonadiabatic equilibrium values calculated at the measured Rayleigh temperatures.

calibrated using laminar flow elements (Meriam Instrument), and these calibrations were repeatable to within ±1% over the range of flows used in the present experiments. The estimated uncertainties in averaged temperature and concentration measurements are illustrated in Fig. 2. Here, averaged results are plotted versus the equivalence ratio for 18 CO/H_2–air flame conditions. The lower values from Table 1 are plotted as error bars. Where no error bars are visible the uncertainty is represented approximately by the size of the plotting symbol. The solid curves in Fig. 2 show results of nonadiabatic equilibrium calculations computed at temperatures representing the average Rayleigh temperature from several calibration sets. These averaged Rayleigh temperatures are about 50 K below adiabatic equilibrium in these calibration flames. The OH calibration is based on independent laser absorption measurements in a CH_4–air flame, and this is consistent with the calculated nonadiabatic equilibrium OH levels in the CO/H_2–air flames, as shown in Fig. 2.

Experiments were conducted on two jet flames with different nozzle diameters but equal Reynolds numbers based on the cold-jet exit conditions. The fuel composition for both flames was 40% CO, 30% H_2, and 30% N_2 by volume. Nozzle dimensions and jet flow conditions are listed in Table 2. The nozzles were constructed from straight tubing with squared-off ends. The thick wall of the tubing provided a small recirculation zone that helped to stabilize

TABLE 2

Nozzle Dimensions and Flow Conditions[a]

Flame	d, Nozzle ID (mm)	Nozzle OD (mm)	U_{jet} (m/s)	Re_{jet}
A	4.58	6.34	76.0 ± 1.5	~16,700
B	7.72	9.46	45.0 ± 0.9	~16,700

[a] $Re = U_{jet}d/\nu$, where $\nu = 2.083 \times 10^{-5}$ m^2/s.

the flames without a pilot. This experimental convenience may lead to computational inconvenience, in that most turbulence models would not be expected to resolve the details of the near-nozzle flow. However, we do not expect this to be a significant liability for these data. The flames were unconfined, and each burner tube was mounted such that the flame base was above the level of the 30-cm by 30-cm exit of the wind tunnel. The coflow air conditions were 0.75 m/s ± 0.05 m/s velocity, 290 K ± 2 K temperature, 0.012 ± 0.002 mole fraction of H_2O vapor, and 100.6 ± 0.4 kPa pressure.

RESULTS AND DISCUSSION

Both flames appeared to be fully attached to the nozzle, and there is no evidence in the data that oxygen is entrained into the fuel jet through extinguished zones near the nozzle. Axial profiles were obtained in both flames and include measurements from $x/d = 20$ to $x/d = 75$ with steps of $5d$, where d is the nozzle inner diameter. Radial profiles were obtained at axial positions of $x/d = 20$, 30, 40, 50, and 60 in each flame. Typically, 800 to 1000 shots were collected at each location in these profiles. Measurements were not taken closer to the nozzle due to considerations of spatial resolution. The smallest scalar length scale, λ_B, was estimated following the approach outlined by Smith et al. [24]. At $x/d = 20$ in the smaller flame the estimated λ_B is approximately equal to the 0.75-mm size of the laser probe volume. Better spatial resolution is achieved further downstream and in the larger flame. There may be some influence of spatial averaging on the measurements, but we would not expect this to alter any of the conclusions of this paper.

The sections that follow report Favre- and conditionally averaged mole fractions of the

measured scalars, as well as several derived quantities based on measured mass fractions. The data base available on the web includes Favre, Reynolds, and conditional statistics of both mole fractions and mass fractions. In addition, the complete files of single-shot mass fractions and mole fractions are available.

Here and in the archived data files the mixture fraction is calculated from the data following the method of Bilger et al. [25].

$$F = \frac{2(Y_C - Y_{C,2})/w_C + (Y_H - Y_{H,2})/2w_H - (Y_O - Y_{O,2})/w_O}{2(Y_{C,1} - Y_{C,2})/w_C + (Y_{H,1} - Y_{H,2})/2w_H - (Y_{O,1} - Y_{O,2})/w_O},$$

where Y's are elemental mass fractions of carbon, hydrogen, and oxygen; w's are atomic weights; and the subscripts 1 and 2 refer to the fuel stream and coflowing air stream, respectively. The fuel and air boundary conditions for the elemental mass fractions are listed in Table 3. Bilger's formulation preserves the stoichiometric value of the mixture fraction, independent of the effects of differential molecular diffusion. The stoichiometric value of the mixture fraction, F_{st}, is 0.295 in the present flames.

Axial and Radial Profiles

Axial (centerline) profiles of Favre-averaged mixture fraction, temperature, and species mole fractions are plotted in Fig. 3 (left side) for the two flames, with the axial coordinate, x, normalized by nozzle diameter, d. In these fully connected flames with low coflow velocity, the scaling by nozzle diameter works well for all measured scalars except for the mole fractions of OH and NO. The OH and NO mole fractions are more strongly influenced by local scalar dissipation and by convective residence time than are temperature and the major species concentrations. Consequently, OH mole fractions are 20–25% lower in flame B than in flame A, and NO levels are about 40% higher. It is this greater sensitivity of some minor species to fluid-dynamic scaling that makes them useful for the evaluation of turbulent combustion models. Axial profiles of scalar fluctuations are also plotted in Fig. 3 (right side). Again, the scaling of axial distance by nozzle diameter demonstrates the similarity of the two flames. Note also that the fluctuations in temperature, H_2O, and CO_2 pass through local minima at the streamwise locations where the corresponding mean values reach their peaks.

Radial profiles of Favre-averaged scalars at streamwise locations of $x/d = 20$ and $x/d = 50$ are plotted in Fig. 4. Again the simple scaling by nozzle diameter works well for temperature and major species in these flames. However, OH levels are lower and NO levels are higher in flame B than in flame A, due to the lower scalar dissipation rates and longer residence times in the larger flame. Axial and radial profiles of the normalized mean and fluctuation of the streamwise component of velocity, as reported by Flury [16], are shown in Figs. 5 and 6 to emphasize the availability of velocity measurements in these flames. The archive [17] of velocity data includes axial profiles and radial profiles at $x/d = 0$, 10, 20, 30, 40, 50, and 60 in each flame.

Axial and radial profiles of velocity and scalars provide an important first level of information on jet flame structure that may be used in the testing and evaluation of turbulent combustion models. However, such profiles yield little information on the details of the relationships among species and the influence of turbulence on scalar transport and reaction progress. Consequently, these profiles are necessary but not sufficient for the establishment of a complete quantitative understanding of the capabilities and limitations of turbulent combustion models, nor are such profiles particularly useful for developing fundamental insights on the effects of turbulence–chemistry interactions. Issues of chemistry and turbulence–chemistry interac-

TABLE 3

Elemental Mass Fraction Boundary Conditions[a]

Stream	Y_C	Y_H	Y_O
Fuel, 1	0.2377	0.0299	0.3167
Coflow, 2	0.0	7.7×10^{-4}	0.2356

[a] Coflow humidity included, CO_2 content in air neglected, balance is N_2.

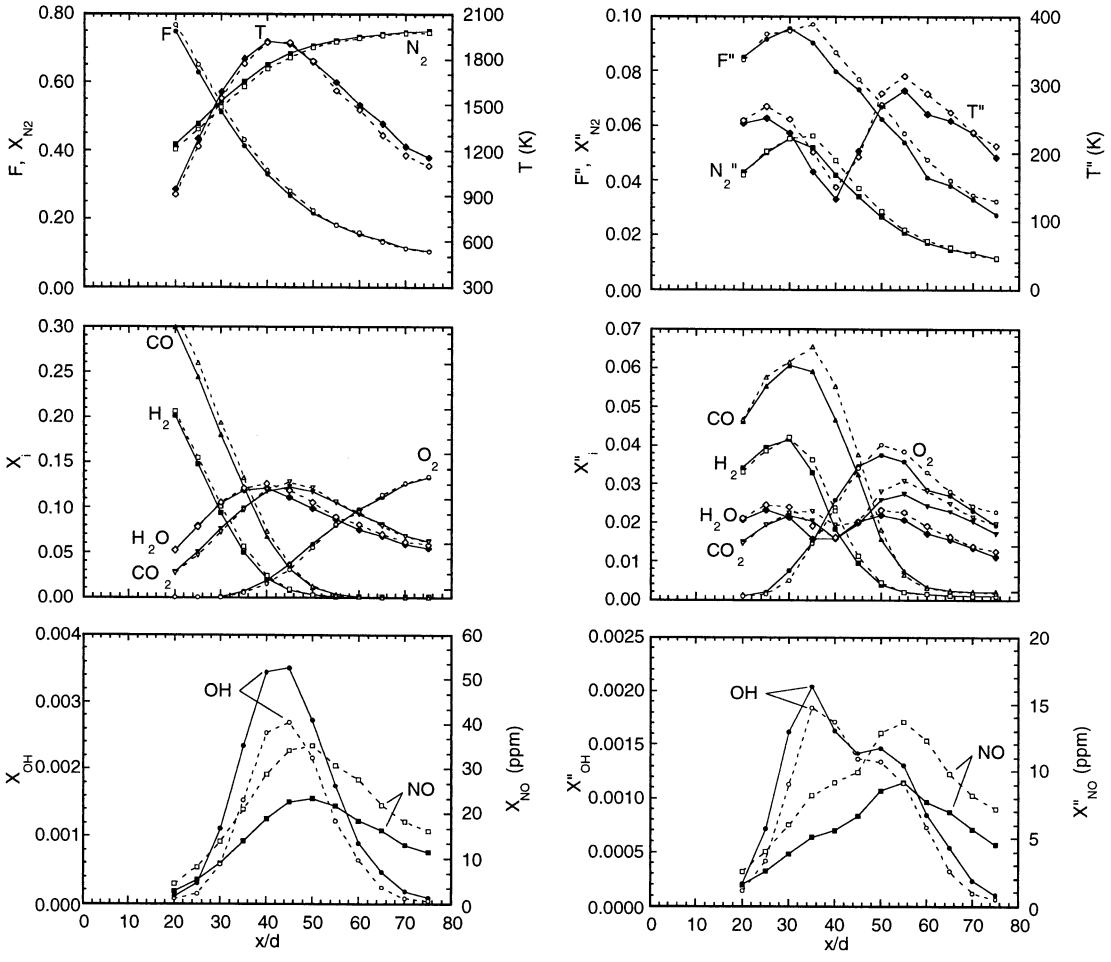

Fig. 3. Axial profiles of Favre-averaged scalars (left side) and rms fluctuations (right side) for the two flames, A (solid lines) and B (dashed lines).

tions may be better explored in mixture-fraction space, as is done in the following sections.

Conditional Statistics and Issues of Scalar Transport

In the present flames there is no evidence of localized extinction at the measured locations or of the entrainment of oxygen into the fuel jet through extinguished or lifted regions at the flame base. This is demonstrated in Fig. 7, which is a scatter plot of temperature and the mole fraction of O_2. In these fully connected flames the scalar structure in mixture-fraction space may be represented conveniently by the conditional mean and rms fluctuation, rather than the complete scatter plots or pdf's. As an illustration, Fig. 8 shows the conditional means of temperature and O_2 mole fraction corresponding to the scatter data in Fig. 7, with the conditional rms fluctuations ($\pm\sigma$) plotted as "error" bars. Conditional statistics presented in this paper are determined using all data from a given radial profile. Previous work has shown some radial dependence of the conditional statistics in hydrogen jet flames, particularly in the upstream region of the flame, and we will consider this detail later in this paper.

Scatter data and conditional means of scalars measured in turbulent flames have often been compared with results of steady, strained, laminar flame calculations. Initial comparisons for

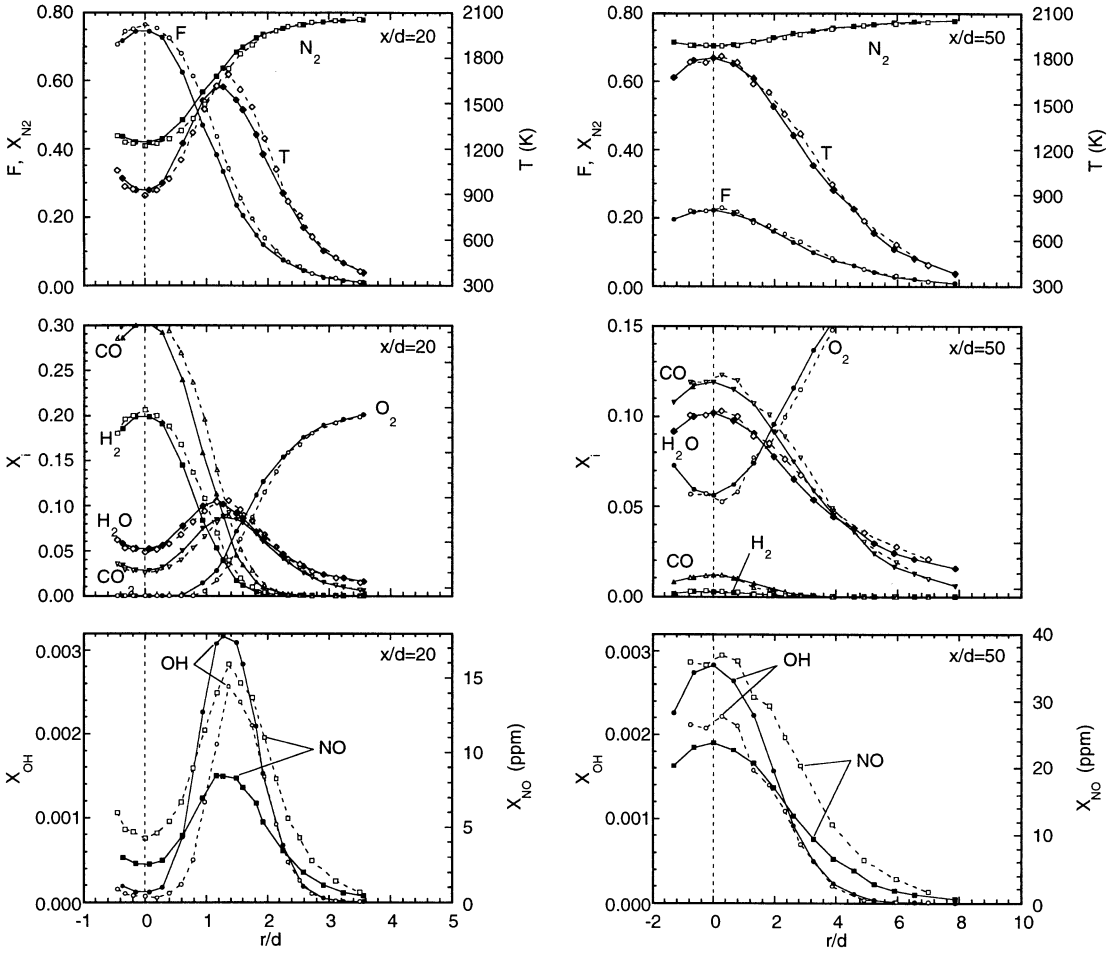

Fig. 4. Radial profiles of Favre-averaged scalars in the two flames, A (solid lines) and B (dashed lines), measured at axial locations $x/d = 20$ (left) and $x/d = 50$ (right). The Favre-averaged stoichiometric flame length is $\sim 44d$ in both flames.

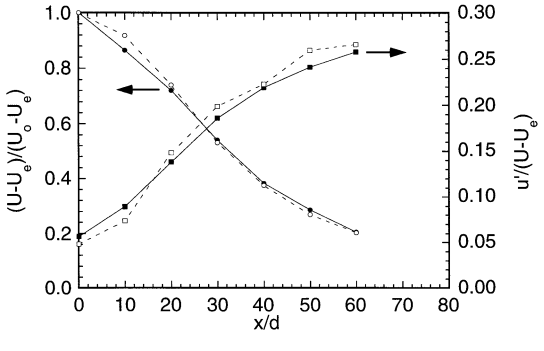

Fig. 5. Centerline profiles of mean and fluctuating axial velocity from LDV measurements by Flury [16] for flames A (solid lines) and B (dashed lines). U_e is the coflow velocity, and U_o is the nozzle exit velocity on the centerline.

these $CO/H_2/N_2$ flames, using the CO mechanism from Peters and Rogg [26], revealed large differences between measurements and laminar calculations that included the Chemkin treatment of species transport. This was true for all measured locations in both turbulent flames. Laminar calculations were repeated with all species diffusivities set equal to the thermal diffusivity, and results of both sets of calculations are shown in Fig. 9. The different treatments of scalar transport result in large differences in the mole fractions of H_2, CO, H_2O, and CO_2. The most obvious effect is that the H_2O/CO_2 ratio decreases by roughly a factor of 2 near the stoichiometric value of the mixture fraction when equal diffusivities are prescribed. Values of scalar dissipation at the stoichiomet-

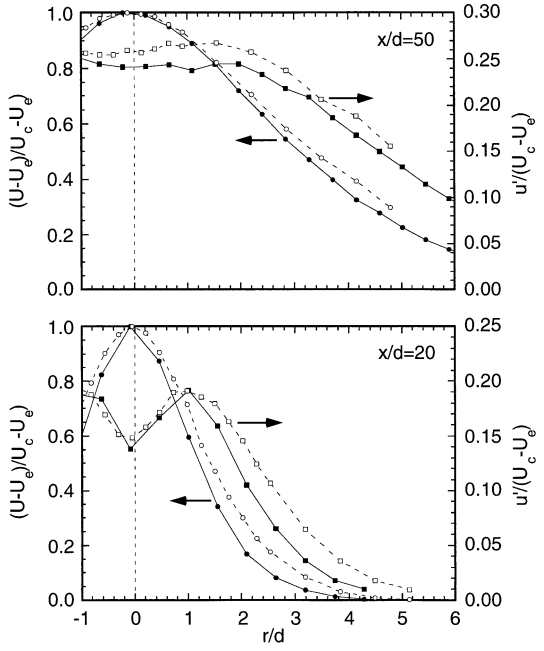

Fig. 6. Radial profiles of mean and fluctuating axial velocity from LDA measurements by Flury [16] for flames A (solid lines) and B (dashed lines) at $x/d = 20$ (lower graph) and $x/d = 50$ (upper graph). U_e is the coflow velocity, and U_c is the axial velocity on the centerline.

ric condition are given in Table 4 for all cases. Note that the scalar dissipation values in the flames with equal diffusivities are about 50% higher than in the corresponding flames with the normal Chemkin treatment of molecular transport. This is related to the fact that, in the presence of differential diffusion, scalar dissipa-

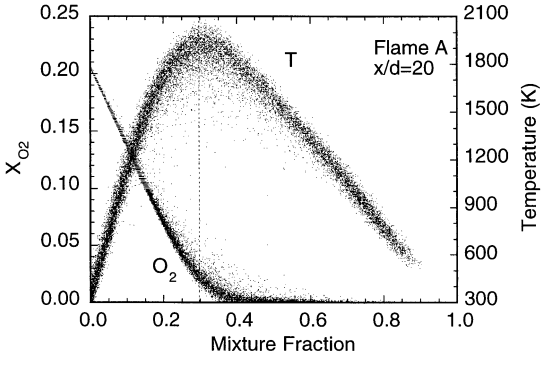

Fig. 7. Scatter plot of single-shot temperature and O_2 measurements in flame A at $x/d = 20$, including approximately 15,000 samples from the complete radial profile. The vertical dashed line indicates the stoichiometric value of the mixture fraction.

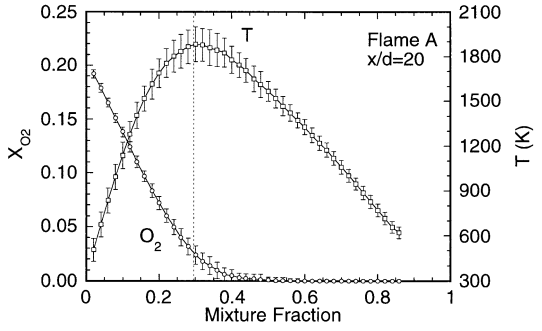

Fig. 8. Conditional mean and rms fluctuation (plotted as uncertainty bars) calculated from the data of Fig. 7, using evenly spaced intervals of 0.02 in mixture fraction. The vertical dashed line indicates the stoichiometric value of the mixture fraction.

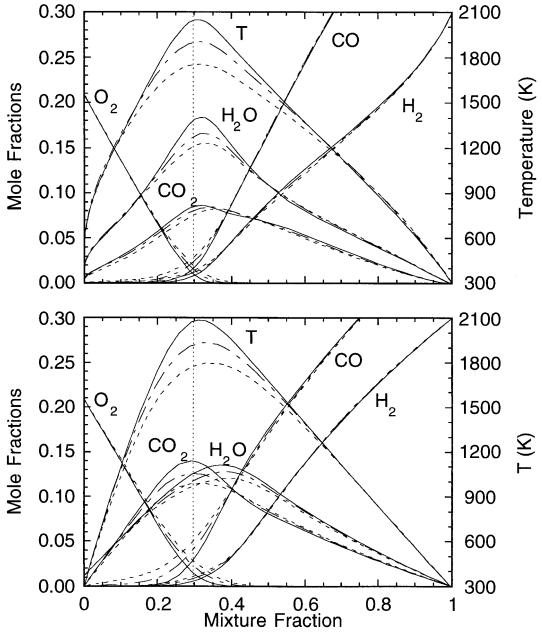

Fig. 9. Results of steady strained opposed-flow laminar flame calculations corresponding to the fuel and air boundary conditions of these turbulent jet flame experiments. Curves for three values of the strain parameter (Tsuji geometry) are plotted in each graph, $a = 10\ s^{-1}$ (solid), 100 s^{-1} (chain-dash), and 400 s^{-1} (dash). Values of the scalar dissipation at the stoichiometric condition in these laminar flames are listed in Table 4. The results in the upper graph include full molecular transport (Chemkin), while the lower graph shows the effect of setting all species diffusivities equal to the thermal diffusivity. The vertical dashed line indicates the stoichiometric value of the mixture fraction.

TABLE 4

Scalar Dissipation Rates at Stoichiometric in the Laminar Flames

Strain Parameter, a (s^{-1})	10	100	400
χ_{st}, Full transport (s^{-1})	3.0	30	120
χ_{st}, Equal diffusivities (s^{-1})	4.6	46	184

tion is sensitive to the definition of mixture fraction.

The equal diffusivity calculations yield better agreement with the measurements. This is illustrated in Fig. 10, which compares measurements from flame A at $x/d = 30$ with the two types of laminar calculations, both with strain parameter $a = 100\ s^{-1}$. Comparison of the measured and calculated H_2O and CO_2 mole fractions near the stoichiometric value of the mixture fraction gives clear evidence of the failure of the laminar flame calculation that includes differential diffusion to approximate the turbulent flame results. Changing the strain rate of the compared flame would not alter this conclusion. The agreement between the equal-diffusivity calculation and the turbulent flame data is remarkable, particularly with regard to the H_2O/CO_2 ratio, suggesting that turbulent stirring has a greater influence than molecular diffusion in determining the major species mole fractions at the jet flame conditions considered here. We would not expect the conditional means in Fig. 10 or the measured H_2O/CO_2 ratio to be altered

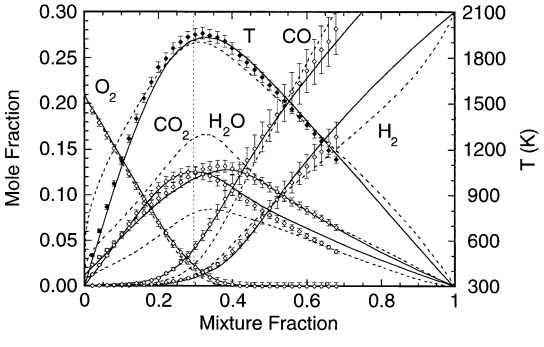

Fig. 10. Measured conditional means at $x/d = 30$ in flame A compared with the two types of laminar calculations for $a = 100\ s^{-1}$: full transport (dash lines) and equal diffusivities (solid lines). Indicated experimental uncertainties correspond to the larger values in Table 1. The vertical dashed line indicates the stoichiometric value of the mixture fraction.

significantly by improved spatial resolution of the measurements because the measurement resolution is already smaller than the estimated smallest scalar length scale at this location.

Figure 11 shows the streamwise evolution of the conditional mean and rms fluctuation of temperature and major species in the two flames. Equal-diffusivity calculations are included in each plot with $a = 10\ s^{-1}$ or $a = 100\ s^{-1}$ depending on which result better approximates the local measurements. (We did not run additional calculations to obtain closer matches at each location.) The values of scalar dissipation at the stoichiometric mixture fraction in these two laminar calculations are $\chi_{st} = 4.6\ s^{-1}$ and $\chi_{st} = 46\ s^{-1}$, respectively. The measurements are consistent with the expected trend of decreasing strain and scalar dissipation rates with increasing streamwise distance. It is also evident that there are greater effects of finite rate chemistry in flame A than in flame B, especially at $x/d = 20$, where the conditional mean temperature is significantly lower in flame A than in flame B. There is some evidence of differential species diffusion in fuel-rich portions of both jet flames. In particular, the measured CO/H_2 ratio in fuel-rich mixtures is somewhat greater than indicated by the equal-diffusivity results. Nevertheless, Figs. 9–11 support the conclusion that for all measured locations in the present flames the equal-diffusivity calculations yield better approximations of the measure conditional means of temperature and the major species mole fractions than do the calculations that include differential diffusion.

The conclusion that turbulent stirring has a greater role than molecular diffusion in determining the conditional mean compositional structure of the present flames is consistent with the results of several experimental, theoretical, and computational studies [e.g., 1, 2, 24, 27–33] that point to a progressive reduction in the effects of differential species diffusion as Reynolds number increases or as one moves downstream in a turbulent jet or flame. Differential-diffusion effects can be strong near the base of a turbulent flame, particularly in cases where H_2 is mixed with a heavier gas in the fuel stream and the cold-jet Reynolds number is in the neighborhood of 10,000 or lower [2]. It appears

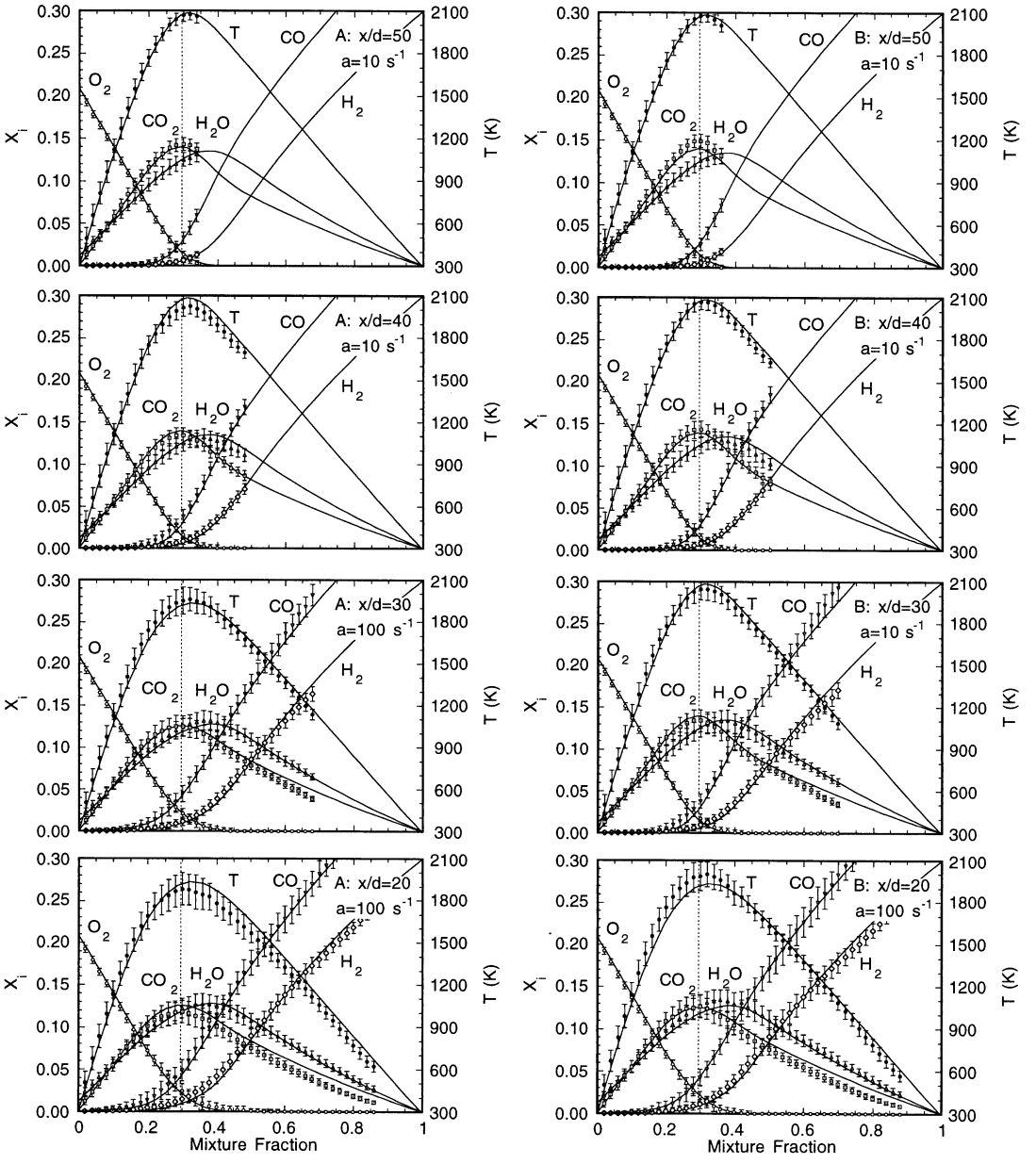

Fig. 11. Streamwise evolution of conditional statistics in the two jet flames. Solid curves show results of equal diffusivity laminar flame calculations at strain rates of $a = 10\ \mathrm{s}^{-1}$ ($\chi_{st} = 4.6\ \mathrm{s}^{-1}$) or $a = 100\ \mathrm{s}^{-1}$ ($\chi_{st} = 46\ \mathrm{s}^{-1}$).

that the Reynolds number is sufficiently high in the present flames to allow turbulent stirring to overshadow or "wash out" the influence of differential diffusion on the conditional means of the major species before the first measurement location of $x/d = 20$ is reached.

The degree of differential diffusion may be quantified by defining and comparing elemental mixture fractions. Here, we define mixture fractions for hydrogen and carbon as:

$$F_H = \frac{Y_H - Y_{H,1}}{Y_{H,2} - Y_{H,1}} \quad \text{and} \quad F_C = \frac{Y_C - Y_{C,1}}{Y_{C,2} - Y_{C,1}},$$

where subscripts 1 and 2 refer to fuel and air streams, respectively. A differential diffusion

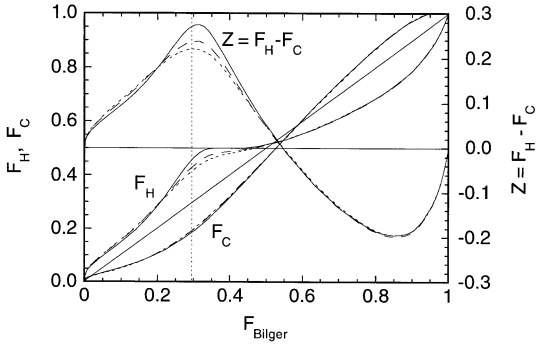

Fig. 12. Elemental mixture fractions, F_H and F_C, and the differential diffusion parameter, z, plotted versus the Bilger mixture fraction. Results are from steady laminar flame calculations with full transport at strain rates of $a = 10\ s^{-1}$ (solid), $100\ s^{-1}$ (long dash), and $400\ s^{-1}$ (short dash).

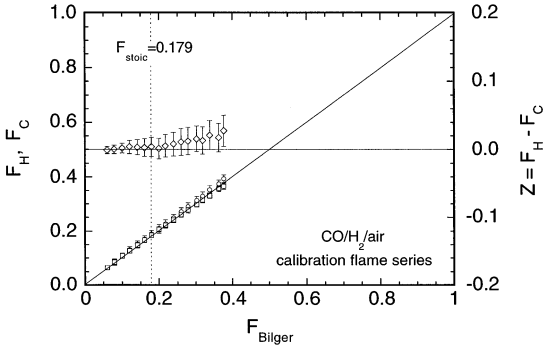

Fig. 13. Mean and rms values of the elemental mixture fractions F_H (squares) and F_C (circles) and the differential diffusion parameter z (diamonds) in the same CO/H_2–air flat flame calibration series as plotted in Figs. 1 and 2. The stoichiometric value of the mixture fraction is lower than in the turbulent flames because there is no N_2 dilution of the fuel.

parameter, $z = F_H - F_C$, can then be calculated as the difference between these elemental mixture fractions. Figure 12 shows calculated results for F_H, F_C, and z plotted versus the Bilger mixture fraction from steady laminar flame calculations using the conventional Chemkin molecular transport package. Preferential diffusion of H_2 toward the reaction zone causes a deficit in hydrogen relative to carbon in region $0.55 < F_{Bilger} < 1$, and there is a positive peak in z just on the rich side of the stoichiometric condition. These calculated flames show strong effects of differential diffusion which are not very sensitive to the applied strain rate.

In the experiments, z is determined by subtracting two uncertain quantities that may have similar values. It is, therefore, important to consider the contributions of random and systematic errors in the differential diffusion results. A relatively simple test is to apply the differential diffusion analysis to measurements from the flat calibration flames, where differential diffusion is expected to be negligible because measurements are made in product gases 3 cm above the burner. Figure 13 shows results for F_H, F_C, and z in each of the CO/H_2/air calibration flames, with mean values shown as symbols and rms fluctuations ($\pm\sigma$) shown as "error" bars. Note that the stoichiometric value of the mixture fraction in the calibration flames is lower than in the turbulent flames ($F_{Bilger} = 0.179$ versus $F_{Bilger} = 0.295$). On the fuel-lean side, where results depend mainly on the H_2O and CO_2 Raman calibrations, z is nearly zero. In fuel-rich flames, where the calibrations for H_2 and CO become increasingly important, z becomes slightly positive. The difference of the averaged z from zero is within the bounds corresponding to the estimated systematic uncertainties for the CO and H_2 Raman measurements. Note that uncertainties in flow meter calibrations, which are typically $\pm 1\%$ for each gas, can contribute to nonzero z values. Results in Fig. 13 indicate that we can expect uncertainties of 0.02 to 0.03 in conditionally averaged values of z in the turbulent flames. Fluctuations in F_H, F_C, and z in the calibration flames are due mainly to shot noise in the species measurements.

Figure 14 shows the streamwise evolution of F_H, F_C, and z in each of the two turbulent flames. Here, again, the symbols show conditional means, and the conditional rms fluctuations are plotted as error bars. Several observations may be made. First, for the turbulent flame conditions and locations considered in the present experiments, the measured effects of differential diffusion are much smaller than in the laminar calculations. Second, the largest differential diffusion effects are observed in the richest samples at each streamwise location, such that the conditional mean z is close to zero for lean and near-stoichiometric samples, but drops toward negative values at the fuel-rich end of each data set. The measured magnitude of z remains small relative to that in the laminar calculations, and it is not completely clear that

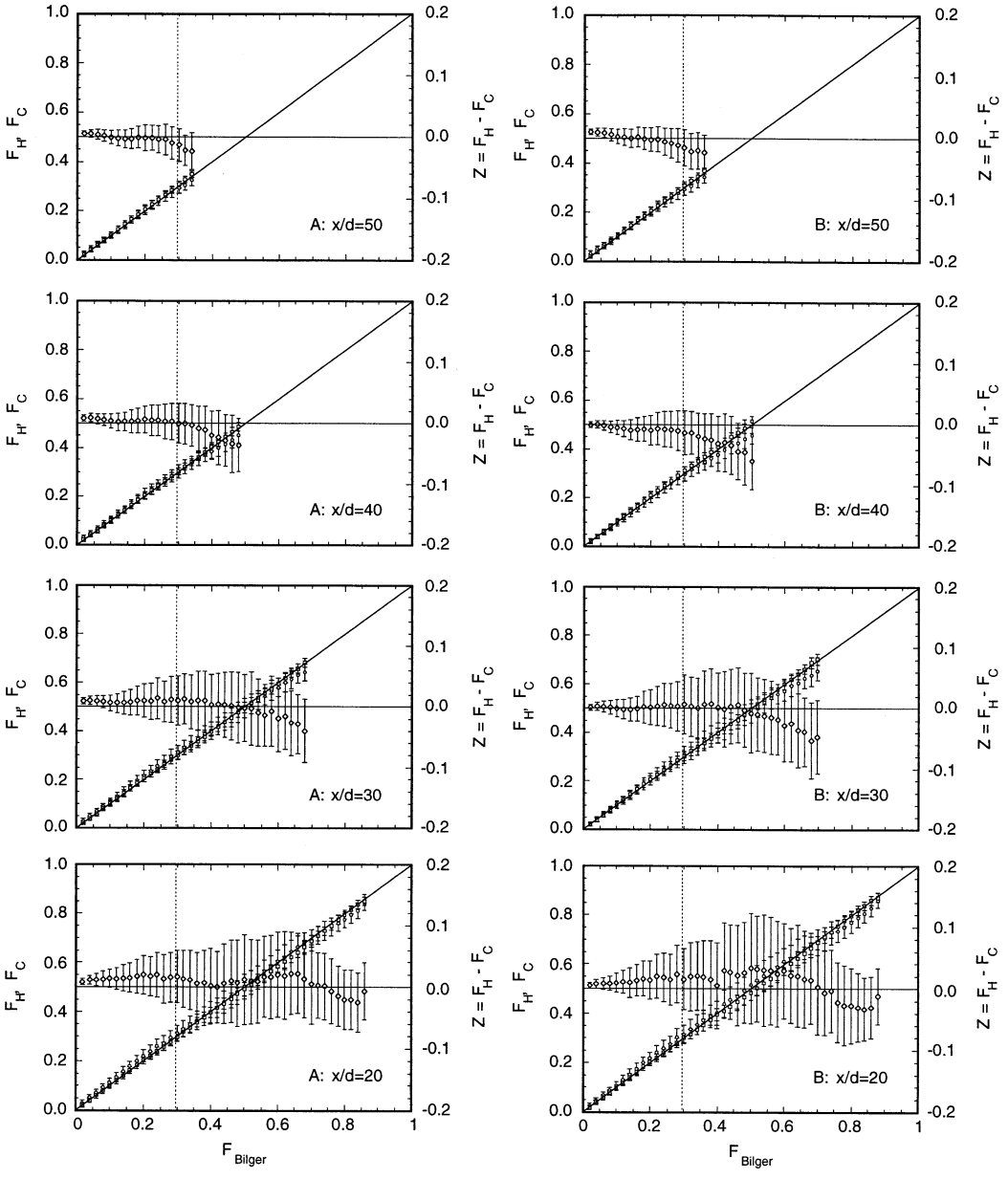

Fig. 14. Streamwise evolution of conditional mean values and rms fluctuations of F_H (squares), F_C (circles), and z (diamonds) in flames A and B. Note expanded scale for z.

the measured streamwise trends in z are significant relative to the accuracy of the measurements. However, the fact that the negative dip in z at the fuel-rich end appears consistently in all plots, with the effect moving across the mixture fraction coordinate, suggests that it is not caused by systematic error in the Raman calibrations or flow meter calibrations. The observed streamwise evolution of the conditional mean of z is believed to reflect a mixing history that involves preferential diffusion of H_2 out of the core of the jet near the flame base [24], where heat release tends to laminarize the flow, particularly at lower Reynolds numbers. Once this initial deficit of hydrogen is created in the richest samples, it appears to be preserved

far downstream because the richest samples at any streamwise location are those which have been least affected by turbulent stirring.

A third observation regarding Fig. 14 is that the conditional fluctuations in z tend to decrease with downstream distance. In fact, the level of fluctuation at $x/d = 50$ is comparable to the noise in measurements above the calibration flames (Fig. 13), and any fluctuations in z that exist near the tips of these jet flames are too small to be measured accurately by the present diagnostics. It is possible to subtract out (approximately) the shot noise contribution to the conditional fluctuations of z, as done by Smith et al. [24]. This procedure is based upon the reasonable assumption that random errors in z are statistically independent of the actual turbulent fluctuations. The noise contribution can then be determined from the rms fluctuations of z obtained from the flat-flame calibration data. However, we have not applied this procedure here.

Larger differential diffusion effects are expected to be present closer to the nozzle, as reported by Meier et al. [2] for nitrogen-diluted H_2 flames and by Bergmann et al. [28] for $CH_4/H_2/N_2$ flames. However, it is clear that the influence of differential diffusion on major species mole fractions is relatively small in the present flames for $x/d \geq 20$ and that turbulent stirring is sufficiently strong to make the effective turbulent diffusivities nearly equal for the measured scalars. One might expect turbulent combustion models built on an assumption of equal diffusivities to perform well in predicting these flames. Conversely, one would expect a flamelet approach to perform poorly if the flamelet library is based on calculations that include full molecular transport.

Trends Related to Damköhler Number

Trends in the conditional means of each measured scalar may be related qualitatively to changes in the relevant Damköhler number ($Da = \tau_{flow}/\tau_{chem}$) between the two flames or among the different locations in a given flame. Such trends have been reported and discussed in many papers. We consider these trends in the context of the present flames not because they provide new fundamental insights but because the quantitative prediction of these results constitutes an important test of submodels for mixing and for the coupling of turbulence and chemistry.

A broad range of chemical reaction rates or time scales is represented by these flames, including the time scales associated with the binary reactions of the H_2/O_2 system, oxidation of CO, decay of OH through the three-body recombination reactions, and formation of NO via the extended Zeldovich mechanism. There is also a broad range of fluid-dynamic time scales in these flames. At the simplest level one might consider the convective residence time from the nozzle to the measurement location (proportional to x/U_{jet}) and the local large-eddy time scale [34–36], which is associated with the large-scale strain rate (and arguably the large-scale turbulent stirring process) and scales as $\tau_{large\text{-}eddy} \propto \delta_{1/2}/(U_c - U_e)$, where $\delta_{1/2}$ is the half-width of the velocity profile.

While it may not be appropriate to assign precise flow and chemical times in turbulent flames, the consideration of Damköhler numbers based on representative time scales can be useful in understanding the potential for coupling between various flow processes and specific reactions or species. Consider CO oxidation as an example. Drake and Blint [37] tabulated chemical time scales (based on peak forward reaction rates) for specific reactions in laminar calculations of $CO/H_2/N_2$ flames with the same fuel volume fractions as used here. For their case with $a = 10\ s^{-1}$, which Fig. 11 has shown to be representative of conditions in portions of the present jet flames, $\tau_{reaction}$ is given as 0.73 ms for the reaction $CO + OH \Leftrightarrow CO_2 + H$. In the present experiments the convective times range from roughly 3 ms ($x/d = 20$, flame A) up to 10's of ms, whereas the local large-eddy times fall in the approximate range of 0.3 ms ($x/d = 20$, flame A) to 5 ms ($x/d = 60$, flame B). Taking $\tau_{chem} \sim 0.73$ ms for CO oxidation and $\tau_{flow} \sim 0.7$ ms from the large-eddy time at $x/d = 20$ in flame B yields $Da_{CO} \sim 1$. This suggests that CO oxidation may be strongly coupled with large-scale mixing processes. Qualitatively, the chemical times for CO oxidation and radical recombination are comparable to flow times within the present flames, the main path for H_2O formation is fast relative

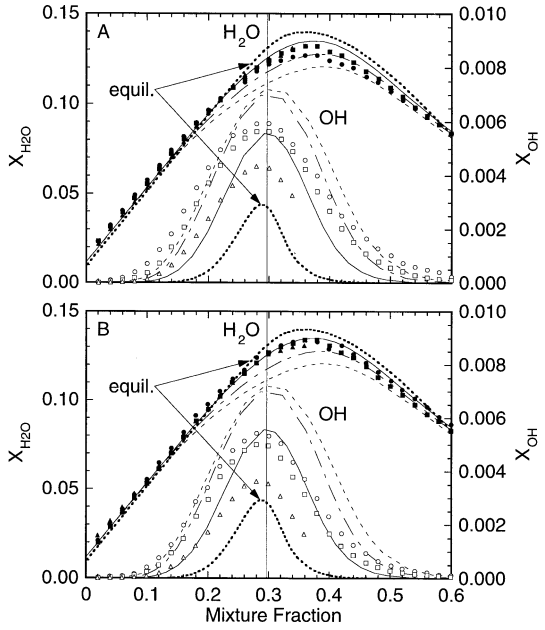

Fig. 15. Conditional means of X_{H_2O} and X_{OH}, in flames A (upper) and B (lower) at streamwise locations $x/d = 20$ (circles), $x/d = 30$ (squares), and $x/d = 50$ (triangles). Curves are plotted for the equal-diffusivity flame calculations at strain rates of $a = 10\ s^{-1}$ (solid), $a = 100\ s^{-1}$ (chain-dash), and $a = 400\ s^{-1}$ (dash). Values of the scalar dissipation at the stoichiometric condition in these three laminar flames are $\chi_{st} = 4.6\ s^{-1}$, $46\ s^{-1}$, and $184\ s^{-1}$, respectively. Adiabatic equilibrium curves (short dash) are included.

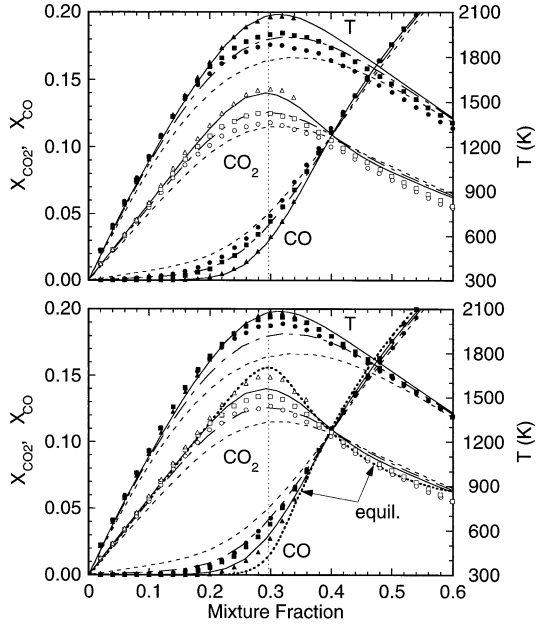

Fig. 16. Conditional means of X_{CO_2}, X_{CO}, and T in flames A (upper) and B (lower) at streamwise locations $x/d = 20$ (circles), $x/d = 30$ (squares), and $x/d = 50$ (triangles). Curves are plotted for the equal-diffusivity flame calculations at strain rates of $a = 10\ s^{-1}$ (solid), $a = 100\ s^{-1}$ (chain-dash), and $a = 400\ s^{-1}$ (dash). Values of the scalar dissipation at the stoichiometric condition in these three laminar flames are $\chi_{st} = 4.6\ s^{-1}$, $46\ s^{-1}$, and $184\ s^{-1}$, respectively. Adiabatic equilibrium curves (short dash) for X_{CO_2} and X_{CO} are included in the lower graph.

to fluid-dynamic times, and thermal formation of NO is relatively slow. These relationships are reflected in the measured conditional means, as discussed below.

Figure 15 shows the measured condition means of the mole fractions of H_2O and OH at streamwise locations of $x/d = 20$, 30, and 50 in each of the two flames A and B. Curves representing adiabatic equilibrium conditions and steady strained laminar flame solutions are also plotted. The laminar flame curves correspond to equal-diffusivity calculations with three values of the strain parameter, $a = 10\ s^{-1}$, $100\ s^{-1}$, and $400\ s^{-1}$ ($\chi_{st} = 4.6\ s^{-1}$, $46\ s^{-1}$, and $184\ s^{-1}$, respectively). The conditional mean of X_{H_2O} is relatively insensitive to location, indicating that H_2O formation via the binary reactions is fast relative to the fluid-dynamic time scales. The relatively small differences in the X_{H_2O} curves are believed to be controlled mainly by progress of the slower radical recombination reactions. The conditional mean of X_{OH} changes significantly from a peak of roughly twice equilibrium at $x/d = 20$ in flame A to roughly 20% above equilibrium at $x/d = 50$ in flame B. This result indicates that the time scales for radical recombination are comparable to time scales of the flow.

Figure 16 includes the corresponding results for CO_2, CO, and temperature. There is a distinct progression in the conditional mean results for X_{CO} and X_{CO_2} as one moves downstream in a given flame or compares flames A and B at a given value of x/d. At $x/d = 20$ in flame A the CO and CO_2 levels are comparable to those in a laminar flame at a moderate strain rate between 100 and 400 s^{-1}. At $x/d = 50$ in flame B the CO and CO_2 results fall between the curves for equilibrium and for the $a = 10\ s^{-1}$ strained laminar flame. Trends in the measured conditional means of CO, CO_2, and OH indicate a strong coupling between flow and reaction (effective Damköhler numbers are of

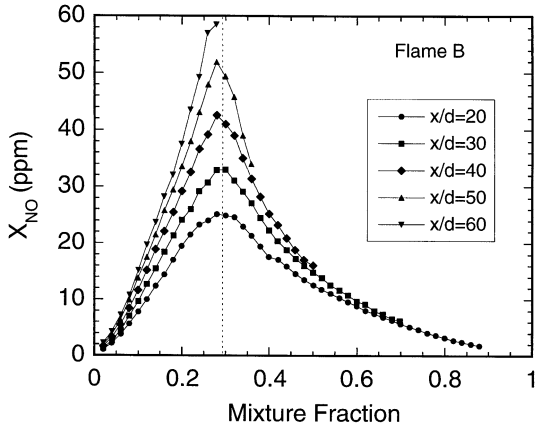

Fig. 17. Streamwise evolution of the conditional mean of nitric oxide mole fraction in flame B.

order unity). Thus, the quantitative prediction of the conditional statistics of these species is expected to be a useful test of submodels for coupling turbulence and chemistry.

Figure 17 shows the measured conditional means of NO mole fraction in flame B. Thermal NO formation is sufficiently slow that NO concentrations remain far below equilibrium everywhere in these flames ($Da_{NO} \ll 1$). Consequently, there is a steady increase in conditional mean NO mole fraction as one moves downstream in each flame, so long as there is some fluid within the NO-forming interval in mixture fraction near the stoichiometric condition.

Radial Dependence of Conditional Means

All of the conditional mean results discussed until now were generated using data from complete radial profiles. Some radial dependence of the conditional statistics is expected in turbulent jet flames, but previous experimental studies have indicated that this dependence is relatively weak. Barlow and Carter [38] examined this issue in hydrogen jet flames and reported that the radial dependence of conditional means of measured scalars was minor in the lower half of the flames and negligible in the upper half. Figure 18 shows conditional mean curves for selected scalars from seven separate radial locations at $x/d = 30$ in flame A. The statistical sample size is limited (typically 30 to 60 samples per mixture-fraction bin), but these data confirm that there is only a relatively weak radial dependence of the measured conditional means at this location in flame A. OH shows the greatest variation, with a spread of about 10% between the different curves near the stoichiomatic mixture fraction and larger percentage differences for fuel-lean conditions.

Near the stoichiometric mixture fraction and at lean conditions, the OH curves in Fig. 18 tend to shift downward as radius increases from 5 mm to 15 mm. This is the region where the radial gradient of the mean axial velocity is steepest. Therefore, larger radius corresponds on average to lower velocity, longer residence time, and more time for the three-body recombination reactions to bring OH levels down toward equilibrium at a given mixture fraction. Thus, the trend in X_{OH} in Fig. 18 is consistent with the effects of Damköhler number discussed above. The curves for X_{CO_2} in Fig. 18 show some separation near the stoichiometric condition, and the CO_2 trend is also qualitatively consistent with changes in Damköhler number. CO_2 mole fraction tends to increase with increasing radius, corresponding to the increase in effective Damköhler number. Curves for the other measured scalars are generally within ±5% of the result based on averaging all data from the full radial profile, and such Damköhler-related trends are less obvious.

The radial dependence of conditional means is slightly greater at $x/d = 20$ in flame A (not shown) than at $x/d = 30$ but less at all other measured streamwise locations in the two flames. These results indicate that for fully connected simple jet flames, such as the present cases, the assumption of radial independence of conditional means is a reasonable approximation. One would not expect significant modeling errors to result from the use of this assumption in the context of conditional moment closure (CMC) calculations of this type of flame. Similarly, in the context of flamelet models, one would not expect significant errors to result from the use of a single value of the scalar dissipation rate to represent the mean scalar values at a given streamwise location. This latter conclusion was already apparent from Fig. 11. At the same time, the data confirm that in this jet flame the radial dependence of conditional means is greater than the axial dependence. For example, a radial displacement of less than one

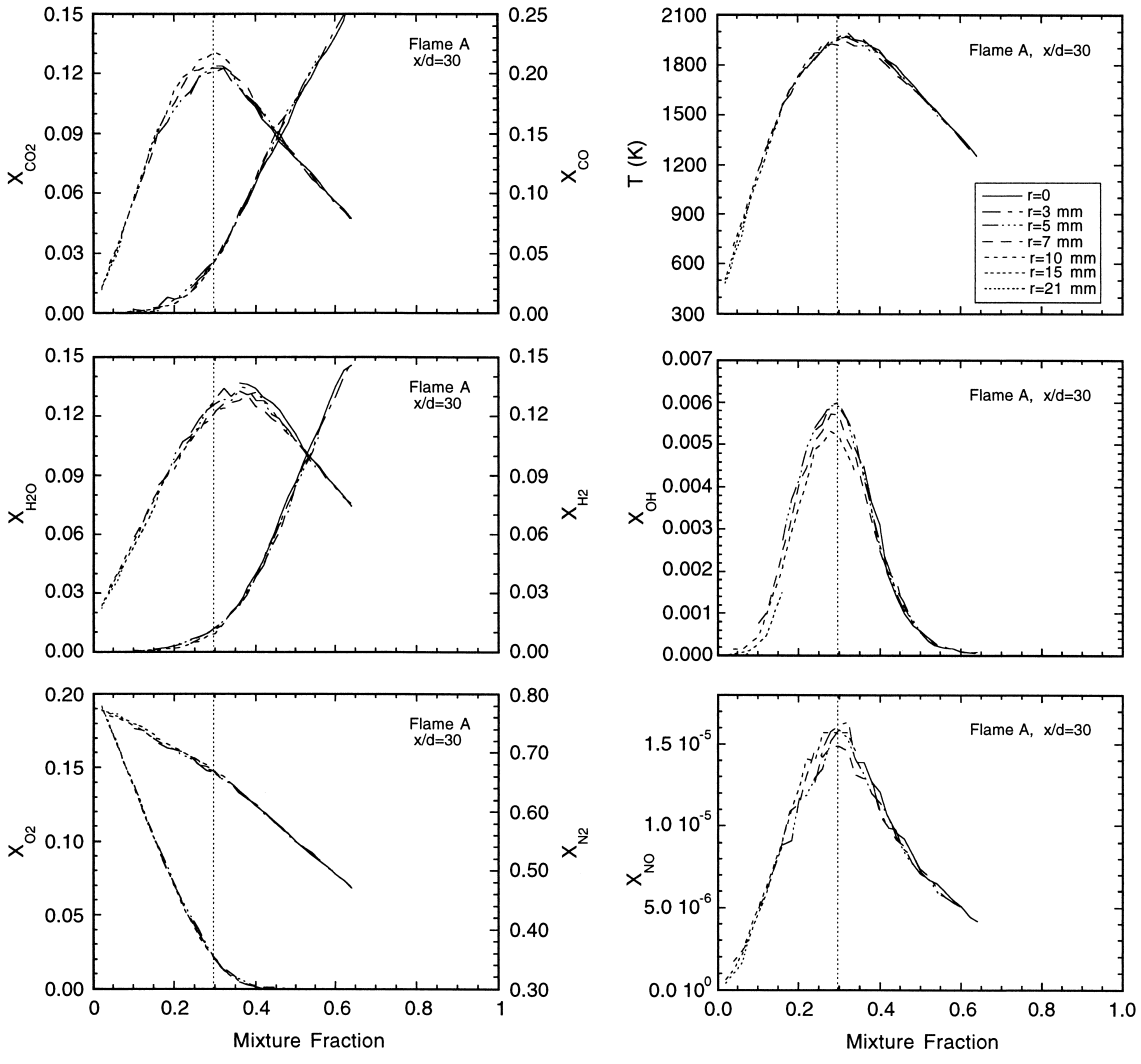

Fig. 18. Conditional means of selected scalars determined at seven separate radial locations at $x/d = 30$ in flame A.

nozzle diameter from $r = 3$ mm to $r = 7$ mm (Fig. 18) causes changes in X_{CO_2} and X_{OH} at the stoichiometric mixture fraction that are comparable to the effects of moving more than 10 times that distance in the axial direction from $x/d = 20$ to $x/d = 30$ (Figs. 16 and 17).

The conditional mean curves in Fig. 18 each span a limited interval in mixture fraction because the mixing characteristics of this flame do not bring all values of the mixture fraction to any single location. Very lean samples do not penetrate to the centerline, and the richest samples do not stray far from the centerline. The pdf's of mixture fraction at each of the radial locations shown in Fig. 18 are plotted in Fig 19. Here, the pdf's are not smooth because of the relatively small sample size of 800–1000 for each location, and they are broadened somewhat by noise, the magnitude of which can be estimated from the calibration results in Fig. 1. However, these pdf's serve to quantify the mixing statistics in these flames, and they provide another important point of comparison with turbulent combustion models. Corresponding pdf's for other locations may be generated from the data base [17], as radial position is tabulated in the single-shot data files.

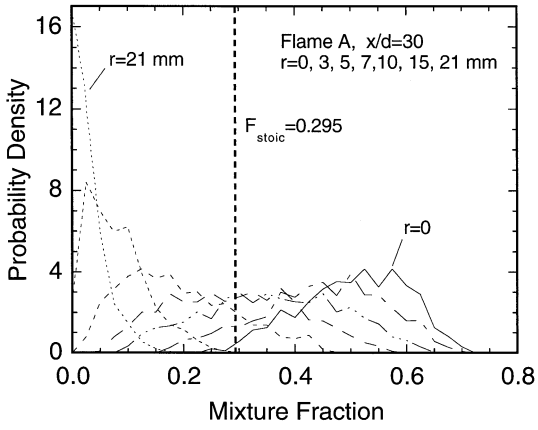

Fig. 19. Pdf's of mixture fraction at the seven locations from Fig. 18.

Deviation from Partial Equilibrium

Partial equilibrium assumptions, when valid, can be useful for combustion models and for the analysis of experimental data because they allow the concentrations of certain species that are not calculated or measured to be derived from those that are. If one or more of the rapid binary reactions

$$H + O_2 \Leftrightarrow OH + O \quad (R1)$$

$$O + H_2 \Leftrightarrow OH + H \quad (R2)$$

$$OH + H_2 \Leftrightarrow H_2O + H \quad (R3)$$

$$OH + OH \Leftrightarrow H_2O + O \quad (R4)$$

$$H_2 + O_2 \Leftrightarrow 2OH \quad (R5)$$

is in equilibrium, then a state of partial equilibrium exists, even if other slower reactions in the system are far from being equilibrated. Note that R5 is the sum of R1 and R2, rather than an elementary reaction in itself.

Partial equilibrium of these reactions in laminar and turbulent flames of various fuels has been considered by many authors [5, 20, 24, 37–41, and references therein]. Detailed laminar flame calculations have indicated that these reactions are equilibrated, or nearly so, only at temperatures above ~1700 K in hydrogen flames and under more restrictive conditions in methane flames. Barlow et al. [20] used reaction R4 to determine O atom concentrations at high-temperature conditions in a turbulent hydrogen jet flame, based on simultaneous measurements of OH, H_2O, and temperature. However, experimental verification of the conditions under which partial equilibrium is achieved is difficult because it requires accurate measurements of temperature and multiple species. Still, quantitative information on deviations from partial equilibrium in turbulent flames is expected to be useful for the process of evaluating models for the coupling of turbulence and chemistry and for understanding the limitations of some reduced mechanisms.

Drake and Blint [37] provide an extensive discussion of the structure of opposed-flow laminar flames of $CO/H_2/N_2$ fuel (same ratios as used here), including effects of differential diffusion, superequilibrium radical formation, and deviations from partial equilibrium. The CO oxidation reaction

$$CO + OH \Leftrightarrow CO_2 + H, \quad (R6)$$

which is slower than the shuffle reactions R1–R5, is an important heat release step in CO and hydrocarbon flames. Combining R6 and R3 yields the water–gas shift reaction

$$CO + H_2O \Leftrightarrow CO_2 + H_2, \quad (R7)$$

in which all species are measured in the present experiments. Drake and Blint [37] observed that the water–gas shift reaction achieved partial equilibrium in laminar calculations of $CO/H_2/N_2$ flames only at low strain rates and for temperatures above 1900 K.

Here we consider deviations from partial equilibrium in the turbulent flames and compare the results with laminar flame calculations at intermediate strain rates, which appear to be representative of conditions within these turbulent flames. For this purpose we define the ratio

$$R_{wg} = ([CO_2][H_2]/[CO][H_2O])/K_{EQ7},$$

where the species concentrations are either measured or taken from the laminar flame calculations and K_{EQ7} is the equilibrium constant for the water–gas shift reaction, R7. R_{wg} is unity when this reaction is equilibrated. An analogous ratio for the shuffle reaction R5 may be defined as

$$R_{sh} = ([OH]^2/[O_2][H_2])/K_{EQ5}.$$

However, we do not report results on R_{sh} in the present turbulent flames because the uncertain-

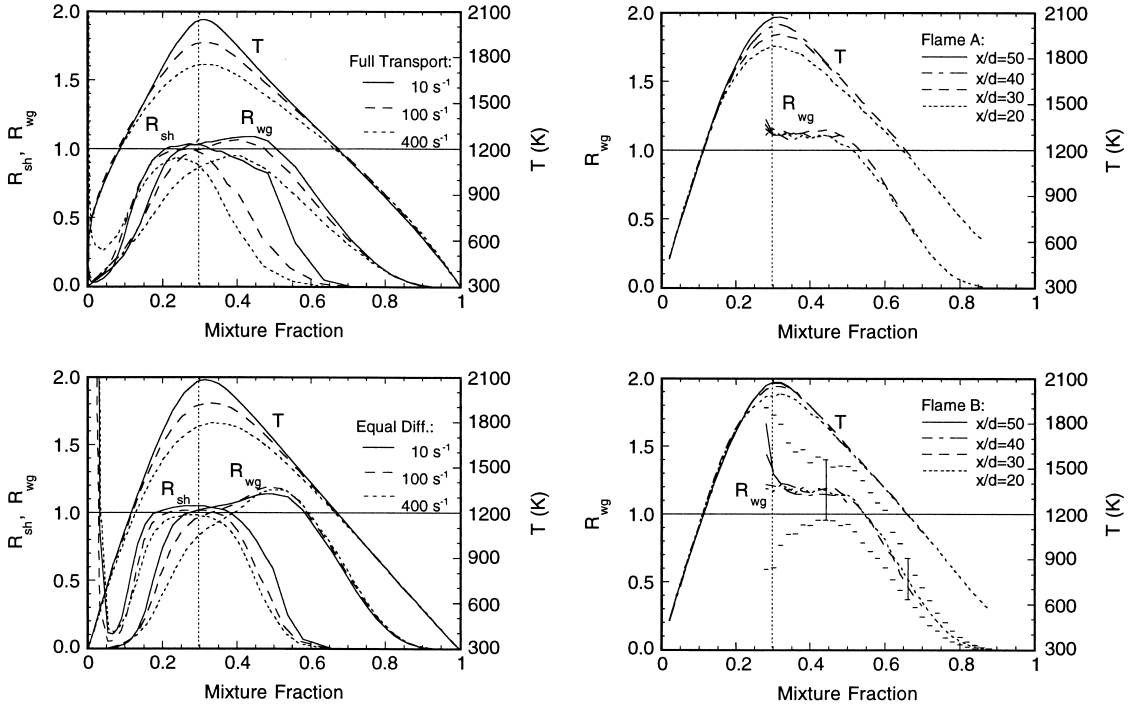

Fig. 20. Results for the partial equilibrium ratios R_{wg} and R_{sh} and the temperature in laminar flame calculations (left) and turbulent flame measurements (right) at the strain rates and streamwise locations indicated. The vertical dashed line corresponds to the stoichiometric value of the mixture fraction.

ties are too large for the results to be quantitatively useful. The reason is that, for all conditions in the present jet flames, at least one of the species, OH, O_2, or H_2, is present only in low concentration.

Figure 20 (left side) shows curves of R_{wg} and R_{sh} versus mixture fraction for laminar flame calculations at strain rates of $a = 10\ s^{-1}$, 100 s^{-1}, and 400 s^{-1}, with full transport and with equal diffusivities. Corresponding curves of temperature are also plotted. (Note that for the full transport calculations the scalar dissipation at the stoichiometric condition depends on the definition of mixture fraction. The Bilger formulation for mixture fraction yields scalar dissipation values in the full transport cases that are roughly 30% lower than those in the equal diffusivity cases.) It is clear that deviations from partial equilibrium in these laminar calculations depend on stoichiometry and transport, as well as on temperature. Consider first the shuffle reaction R5. Taking 10% deviation of R_{sh} from unity as an arbitrary criteria for departure from equilibrium, it is apparent that partial equilibrium of R5 holds over a wider temperature range when all species diffusivities are set equal to the thermal diffusivity. Regardless of the transport assumption, partial equilibrium of R5 holds to a lower temperature on the fuel-lean side than on the fuel-rich side. On the fuel-rich side there are significant differences between the curves for the full-transport and equal-diffusivity calculations. The graphs on the right side of Fig. 20 show the conditional mean curves of R_{wg} in turbulent flames A and B at streamwise locations of $x/d =$ 20, 30, 40, and 50. R_{wg} is not plotted for fuel-lean mixture fractions because concentrations of CO and H_2 become too low to be measured with useful accuracy. The conditional rms fluctuations in R_{wg} at $x/d = 40$ are plotted as error bars ($\pm\sigma$), and it is apparent that these fluctuations increase rapidly as CO and H_2 disappear near the stoichiometric mixture fraction.

In Fig. 21 the same results for R_{wg} in the laminar and turbulent flames are plotted versus temperature. The temperature coordinate make even more obvious the influences of stoichiometry and transport on departures from equilib-

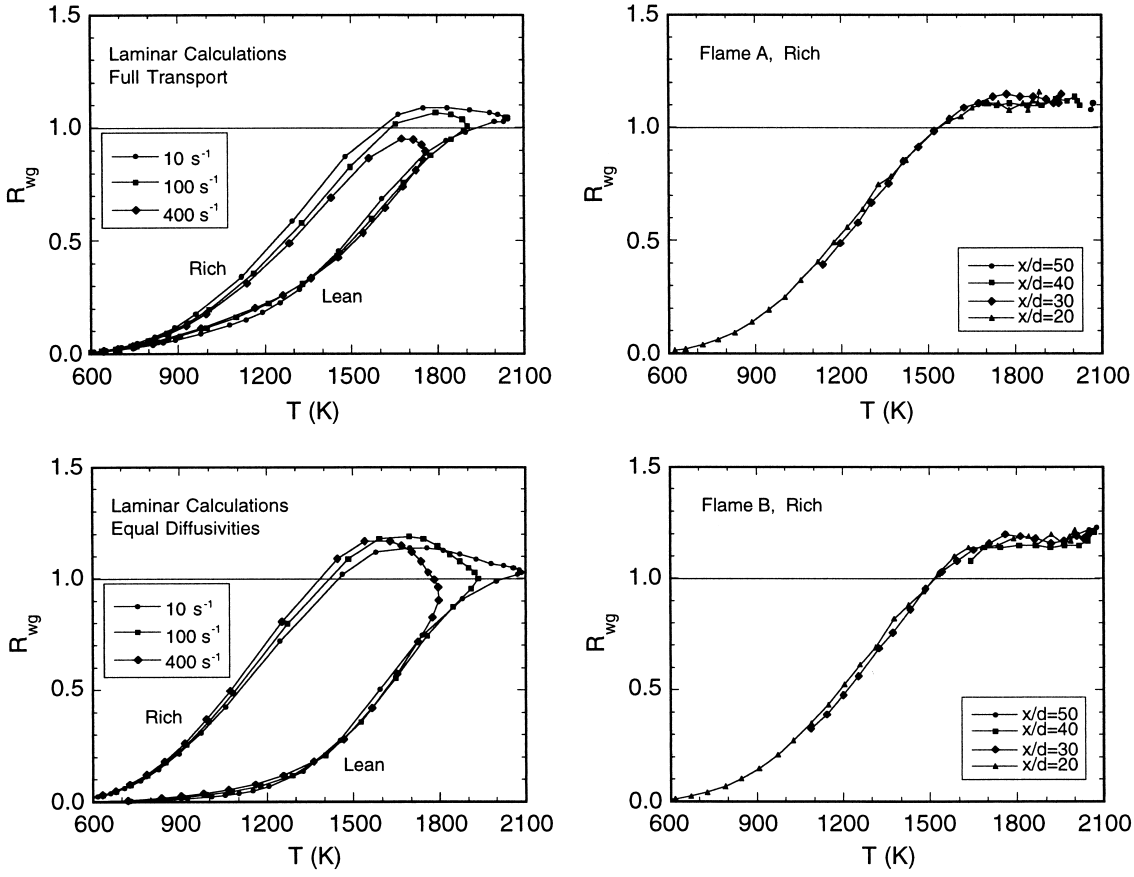

Fig. 21. Results for R_{wg} plotted vs. temperature for laminar flame calculations (left) and turbulent flame measurements (right). Only fuel-rich results are plotted for the turbulent flames.

rium of the water–gas shift reaction in the laminar flame calculations. There are distinct lean and rich legs, and the curves are quite different for the two transport scenarios. There is not a clear asymptotic trend toward partial equilibrium ($R_{wg} = 1$) at the highest temperatures for the strain rates covered by these laminar calculations.

Systematic uncertainty in the conditional means of R_{wg} may be estimated at selected points based on the individual uncertainties in Table 1 and the sensitivity of the equilibrium constant to error in the conditional mean temperature. Errors in species and temperature are assumed to be independent for this purpose. For the conditions in flame A at $x/d = 30$ and 0.4 mixture fraction the uncertainty in R_{wg} is estimated to be $\pm$ 9% or about $\pm$ 0.01, based on lower values from Table 1. At a mixture fraction of 0.6, the estimated uncertainty in R_{wg} roughly doubles because temperatures are in the middle of the range where the CO and H_2 calibrations are interpolated and the higher uncertainties in Table 1 apply. Uncertainty in R_{wg} also increases as mixture fraction approaches the stoichiometric condition and the concentrations of CO and H_2 become small. This trend is most obvious in Fig. 20 at the fuel-lean ends of the curves for $x/d = 40$ and $x/d = 50$ in flame B, where scalar dissipation rates are lowest. Away from the stoichiometric condition, the relative uncertainty in comparing curves at different streamwise locations in the same flame depends on calibration drift and is expected to be below 5%.

Within the limits imposed by these experimental uncertainties, there are a few observations to be made regarding the conditional mean results for R_{wg} in the turbulent flames. First, there is no significant streamwise evolution within each flame in the partial-equilibrium

behavior of the water–gas shift reaction. Second, R_{wg} reaches a plateau between 1.1 and 1.2 at temperatures above 1700 K. The failure of the measured values to approach unity at the highest measured temperatures may result from errors in background and crosstalk corrections that become important when concentrations of CO and H_2 become small. Third, with the exception of these near-stoichiometric results, the conditional means from the turbulent flames fall between the curves for the full-transport and equal-diffusivity calculations. Finally, partial equilibrium of the water–gas shift reaction does not appear to be a good approximation for these jet flames. If it is achieved at all (within 10%), partial equilibrium of the water–gas shift reaction will only hold for a small fraction of conditions in these flames.

CONCLUSIONS

Detailed scalar measurements have been reported for two simple turbulent jet flames of $CO/H_2/N_2$ fuel (40%/30%/30%) having the same Reynolds number of 16,700 but different nozzle diameters. The flames are both fully attached, and there is no evidence of localized extinction at the measured locations or of the penetration of oxygen into the jet core due to lift off or extinction near the flame base. These results, combined with the three-component velocity measurements reported separately by Flury [16], are believed to constitute the most complete data set available for this type of flame. With regard to the systematic evaluation of turbulent combustion models, these geometrically simple flames represent a modest increment in chemical kinetic complexity over hydrogen jet flames, and they may be addressed by a wide range of nonpremixed combustion models. The complete data archives, including both mole fractions and mass fractions, have been made available on the Internet to facilitate comparisons with model calculations. Aspects of the measured results have been presented and discussed in terms of their relevance to the testing of turbulent combustion submodels. The main conclusions of this study are as follows:

Axial and radial profiles of Favre-averaged temperature and major species mole fractions are similar when distance is scaled by the nozzle diameter. However, at a given streamwise distance, x/d, the OH levels are lower and the NO levels are higher in the larger flame, due to the lower scalar dissipation rates and longer residence times.

Comparisons with two types of laminar flame calculations have shown that the conditional means of major species mole fractions in the turbulent flames are better approximated by laminar flame calculations that prescribe equal diffusivities. This indicates that turbulent stirring has a greater influence than molecular diffusion in determining major species mole fractions for the flow conditions and measurement locations considered in the present experiments.

Analysis of elemental mixture fractions of hydrogen and carbon and of the differential diffusion parameter z, defined as the difference between these elemental mixture fractions, has confirmed that differential diffusion effects in the turbulent flames are small compared to those in laminar flames computed with the usual Chemkin treatment of molecular transport.

The streamwise evolution of conditional means of CO, CO_2, and OH in each flame, as well as the differences in the two flames between conditional means of these species at a given streamwise location, x/d, indicate a strong coupling between time scales of the flow and time scales of the reactions that control departure of these species from equilibrium (effective Damköhler number of order unity). Thus, the quantitative prediction of conditional statistics of CO, CO_2, and OH in these flames is expected to be a useful test of submodels for coupling turbulence and chemistry.

There is some radial dependence of the conditional means of measured scalars in these flames, and this dependence is consistent with considerations of the effective Damköhler numbers of the reactions controlling those species. However, the radial variations in conditional means remain relatively small, such that statistics based on data from a complete profile yield a reasonable representation of scalar structure.

Partial equilibrium of the water–gas shift reaction is not achieved in these flames (greater than 10% deviation), except perhaps in the small fraction of samples corresponding to the highest temperatures.

Work at Sandia was supported by the United States Department of Energy, Office of Basic Energy Sciences. C.D.C. was supported by the AFOSR under Air Force Contract F33615-92-2202. Informative discussions with R. Bilger, G. Kosály, and H. Pitsch during the preparation of this paper are gratefully acknowledged. Velocity measurements by M. Flury at ETH Zurich were supported by the Bundesamt für Energiewirtschaft.

REFERENCES

1. Barlow, R. S., and Carter, C. D., *Combust. Flame* 97:261–280 (1994); and *Combust. Flame* 104:288–299 (1996).
2. Meier, W., Vydorov, A. O., Bergmann, V., and Stricker, W., *Appl. Phys. B* 63:79–90 (1996).
3. Neuber, A., Krieger, G., Tacke, M., Hassel, E. P., and Janicka, J., *Combust. Flame* 113:198–211 (1998).
4. Web site of the International Workshop on Measurement and Computation of Turbulent Nonpremixed Flames, www.ca.sandia.gov/tdf/Workshop.html, includes data archives, information on computational submodels, and results of collaborative comparisons of measured and modeled results for various turbulent flames.
5. Chen, J.-Y., Chang, Y.-C., and Koszykowski, M., *Combust. Sci. Technol*. 110:505 (1996).
6. Barlow, R. S., Smith, N. S. A., Chen, J.-Y., and Bilger, R. W., *Combust. Flame* 117:4–31 (1999).
7. Schlatter, M., Ferreira, J. C., Flury, M., and Gass, J., *Twenty-Sixth Symposium (International) on Combustion*, The Combustion Institute, Pittsburgh, 1996, pp. 2215–2222.
8. Strahle, W. C., *Prog. Energy Combust Sci*. 12:253–255 (1986).
9. Faeth, G. M., and Samuelsen, G. S., *Prog. Energy Combust Sci*. 12:305–372 (1986).
10. Drake, M. C., and Kollmann, W., *Prog. Energy Combust. Sci*. 12:373–392 (1986).
11. Masri, A. R., Dibble, R. W., and Barlow, R. S., *Prog. Energy Combust. Sci*. 22:307–362 (1996).
12. Masri, A. R., and Dibble, R. W., *Twenty-Second Symposium (International) on Combustion*, The Combustion Institute, Pittsburgh, 1988, pp. 607–618.
13. Correa, S. M., and Gulati, A., *Twenty-Second Symposium (International) on Combustion*, The Combustion Institute, Pittsburgh, 1988, pp. 599–606.
14. Correa, S. M., and Gulati, A., *Combust. Flame* 89:195–213 (1992).
15. Masri, A. R., Dibble, R. W., and Barlow, R. S., *Combust. Flame* 91:285–309 (1992).
16. Flury, M., Ph.D. thesis and paper in preparation, ETH Zurich, Switzerland.
17. $CO/H_2/N_2$ jet flame data base under Experimental Data Archives on the web site for the International Workshop on Measurement and Computation of Turbulent Nonpremixed Flames, www.ca.sandia.gov/tdf/Workshop.html.
18. Carter, C. D., and Barlow, R. S., *Optics Lett*. 19:299–301 (1993).
19. Nguyen, Q. V., Dibble, R. W., Carter, C. D., Fiechtner, G. J., and Barlow, R. S., *Combust. Flame* 105:499–510 (1996).
20. Barlow, R. S., Fiechtner, G. J., and Chen, J.-Y., *Twenty-Sixth Symposium (International) on Combustion*, The Combustion Institute, Pittsburgh, 1996, pp. 2199–2205.
21. Paul, P. H., *JQSRT* 51:511–524 (1994).
22. Paul, P. H., Gray, J. A., Durant Jr., J. L., and Thoman Jr., J. W., *AIAA J*. 32:1670–1675 (1994).
23. Barlow, R. S., and Frank, J. H., *Twenty-Seventh Symposium (International) on Combustion*, The Combustion Institute, Pittsburgh, 1998, pp. 1087–1095.
24. Smith, L. L., Dibble, R. W., Talbot, L., Barlow, R. S., and Carter, C. D., *Combust. Flame* 100:153–160 (1995).
25. Bilger, R. W., Stårner, S. H., and Kee, R. J., *Combust. Flame* 80:135–149 (1990).
26. Peters, N., and Rogg, B., *Reduced Mechanisms for Applications in Combustion Systems*, Springer-Verlag, Heidelberg, 1993.
27. Bilger, R. W., and Dibble, R. W., *Combust. Sci. Technol*. 28:161–172 (1982).
28. Bergmann, V., Meier, W., Wolff, D. and Stricker, W., *Appl. Phys. B* 66:489–502 (1998).
29. Dally, B. B., Masri, A. R., Barlow, R. S., and Fiechtner, G. J., *Combust. Flame* 114:119–148 (1998).
30. Kerstein, A. R., *J. Fluid Mech*. 216:411–435 (1990).
31. Kosály, G., Personal communication of notes on "Mixture fraction based closure models of turbulent nonpremixed combustion," May 1997.
32. Nilsen, V., and Kosály, G., *Combust. Flame* 117:493–513 (1999).
33. Pitsch, H. "Unsteady Flamelet Modeling of Differential Diffusion in Turbulent Diffusion Flames," submitted to *Combust. Flame*.
34. Barlow, R. S., Dibble, R. W., Chen, J.-Y., and Lucht, R. P., *Combust. Flame* 82:235–251 (1990).
35. Mungal, M. G., and Frieler, C. E., *Combust. Flame* 71:23–34 (1988).
36. Broadwell, J. E., and Mungal, M. G., *Twenty-Second Symposium (International) on Combustion*, The Combustion Institute, Pittsburgh, 1988, pp. 579–587.
37. Drake, M. C., and Blint, R. J., *Combust. Sci. Technol*. 61:187–224 (1988).
38. Barlow, R. S., and Carter, C. D., *Combust. Flame* 104:288–299 (1996).
39. Warnatz, J., Maas, U., and Dibble, R. W., *Combustion*, Springer-Verlag, Berlin, 1996.
40. Smyth, K. C., and Tjossem, P. J. H., *Combust. Flame* 79:366–380 (1990).
41. Barlow R. S., Dibble, R. W., Stårner, S. H., and Bilger, *Twenty-Second Symposium (International) on Combustion*, The Combustion Institute, Pittsburgh, PA, 1988, pp. 579–587.

Received 15 January 1999; revised 20 August 1999; accepted 26 August 1999